Sensors and Actuators Reports 8 (2024) 100235

Contents lists available at ScienceDirect

Sensors and Actuators Reports

journal homepage: www.sciencedirect.com/journal/sensors-and-actuators-reports

Size-controlled synthesis of cobalt phosphide (Co_2P) nanoparticles and their application in non-enzymatic glucose sensors via a carbon fiber/Co_2P composite

Tania P. Brito [a], Nicole Butto-Miranda [c], Andrónico Neira-Carrillo [c], Claudia Yáñez [a,e], Soledad Bollo [a,d,*], Domingo Ruíz-León [b,*]

[a] Centro de Investigación de Procesos Redox (CiPRex), Facultad de Ciencias Químicas y Farmacéuticas, Universidad de Chile
[b] Laboratorio de Fisicoquímica y Electroquímica del Estado Sólido, Facultad de Química y Biología, Universidad de Santiago de Chile
[c] Departamento de Ciencias Biológicas Animales, Facultad de Ciencias Veterinarias y Pecuarias, Universidad de Chile
[d] Departamento de Química Farmacológica y Toxicológica, Facultad de Ciencias Químicas y Farmacéuticas, Universidad de Chile, Sergio Livingstone 1007, Independencia, Santiago P.O. Box 233, Chile
[e] Departamento de Química Orgánica y Fisicoquímica, Facultad de Ciencias Químicas y Farmacéuticas, Universidad de Chile, Sergio Livingstone 1007, Independencia, Santiago P.O. Box 233, Chile

ARTICLE INFO

Keywords:
Cobalt phosphide
Enzyme-free glucose sensors
Electrochemical sensors
Carbon fibre composite

ABSTRACT

In this study, we synthesized Co_2P nanoparticles using a solid-state phosphorization method and evaluated the electrocatalytic response to glucose oxidation reaction (GORs). The influence of synthesis conditions on the particle size, morphology of Co_2P species and formation of byproducts is discussed. A lower molar ratio of the phosphorus precursor leads to a decrease in the generation of byproducts. In addition, the calcination temperature and time greatly influence the purity level of the Co_2P species and its particle size. Thus, we obtained three pure Co_2P nanoparticles with different sizes and morphologies. Significant differences in their electrocatalytic activity against the GOR are observed depending on the size of the particles, being the smaller ones the most efficient. Based on Tafel analysis, a higher catalytic activity was observed for the carbon fibre (CF)/Co_2P composite compared to Co_2P, which presented a greater onset potential and low response in current density. Tafel slopes close to 120 mV/dec were obtained for both materials, indicating that the mechanism is independent of the type of Co_2P-based material used. Finally, the performance of the GCE/CF/Co_2P sensor was demonstrated by amperometric measurements, with a sensitivity of 409 $\mu A m M^{-1} cm^{-2}$, a linear range between 39.4 μM and 150 μM, and a detection limit of 0.97 μM, analytical characteristics better than those obtained for other cobalt phosphide-based sensors reported in the literature. In addition, the GCE/CF/Co_2P sensor shows excellent selectivity and demonstrated to be competitive compared to other Co-based non-enzymatic glucose sensors.

1. Introduction

Diabetes mellitus (DM) is a chronic systematic metabolic disease characterized by an unusual increase in blood glucose concentration, that can produce multiple health complications [1,2]. It is one of the most common global diseases and is the main cause of death and disability worldwide [3]. Thus, the adequate control, the prevention of the disease, the existence of reliable methods to quantify glucose in physiological media (blood, saliva, sweat, and tears) are essential [4]. On the other hand, glucose detection is also necessary in other fields, such as quality control in food industries [5,6]. Therefore, highly sensitive, selective, stable, and economical devices for glucose quantification are highly required. Different glucose sensing techniques, such as fluorescence [7], colorimetry [8], electrochemiluminescence [9], and electrochemistry [10,11], have been explored. Non-enzymatic electrochemical sensors have received great attention due to their fast response, high sensitivity and low detection limits; in addition, compared to enzymatic electrochemical sensors, non-enzymatic electrochemical sensors are more stable [12–14].

Transition metal-based materials (especially Ni, Co, and Cu), such as oxides [15], hydroxides [16], sulfides [17], nitrides [18], and phosphides [19,20], have been extensively studied for the development of

* Corresponding authors.
E-mail addresses: sbollo@ciq.uchile.cl (S. Bollo), domingo.ruiz@usach.cl (D. Ruíz-León).

https://doi.org/10.1016/j.snr.2024.100235
Received 18 January 2024; Received in revised form 3 June 2024; Accepted 7 August 2024
Available online 16 August 2024

non-enzymatic glucose sensors due to their abundance, stability, wide variety of syntheses, and great electrocatalytic activity for glucose oxidation. Among these materials, transition metal phosphides (TMP) have attracted attention due to their good electronic conductivity, high thermal and chemical stability, and excellent electrocatalytic activity towards the hydrogen evolution reaction (HER) [21,22] and the oxygen reduction reaction (ORR) [23]. They have been used for supercapacitors [24], batteries [25], and electrochemical detection methods, including glucose detection through non-enzymatic sensors [19,26,27]. Recently, composites with cobalt phosphide species, such as CoP NA/TM [28], CoP/Co-BP [29], and Co_2P/NPCNT [30], have been used in non-enzymatic glucose sensors; which exhibit high sensitivity, low detection limits, and wide linear ranges. However, studies on specific Co_2P species are limited. D. Das et al.[30] reported the catalytic performance of Co_2P-based sensors for glucose electrochemical detection. Considering that metal-rich metal phosphides are usually semiconductors or even superconductors because metal-metal bonds may be present in their structure [21,31], the evaluation of the catalytic activity of Co_2P species in glucose electrooxidation reactions is interesting. Regarding the improvement in the catalytic activity properties of the material, our group recently demonstrated the synergistic effect of carbon fibers (CFs) in a CF/Ni_2P composite [19], suggesting that carbon fibres are a valuable alternative for enhancing catalytic performance in conjunction with Co_2P, increasing surface area and improving sensor electronic transfer.

Solid-state synthesis methods involving thermal decomposition of hypophosphite precursors have been successfully used to generate metal phosphides [32,33], including Co_2P [34], which involves the formation of phosphine gas (PH_3) as an active phosphorus species for reducing metal salts (oxides, hydroxides, chlorides) at high temperatures and in an inert atmosphere. In a highly reducing environment, Co_2P and different species can be formed, so the synthesis of pure Co_2P without the presence of other subproducts is a real challenge. In this sense, W. Peng *et al.* studied how the molar ratio of NaH_2PO_2 to $CoCl_2$ precursors affects Co_2P synthesis [34] and found that the molar ratio of NaH_2PO_2 to $CoCl_2$ influences the formation of Co_2P and impurities. However, other important parameters are the calcination temperature and time, which were studied in the formation of Ni_2P by Q. Guan [33]; where they mention that proportions of P and Ni between 1.5 and 1.75 are indicated for the formation of Ni_2P without appreciable interferents formation by the XRD analysis. Furthermore, the study of calcination temperature between 250 and 350°C and calcination time between 10 and 90 minutes does not influence the formation of interferences, choosing for its synthesis 300°C as temperature and 30 minutes as calcination time. On the other hand, regarding the production of Co_2P, the effect of heating time was studied by applying a one-pot synthesis technique using tri-n-octylphosphine (TOP) [35] and by thermal decomposition method with triphenylphosphine (TPP) [24] as a precursor of phosphorus. In these investigations, relationships between the heating time and the morphology and particle size of the species were observed; however, these relationships have not been studied for Co_2P synthesis by thermal decomposition of hypophosphite precursors.

As Co_2P is an interesting catalytic material in many applications, obtaining pure Co_2P is important for the application in different fields. Therefore, this work examined the effect of important parameters on Co_2P synthesis by phosphorization methods, such as the molar ratio between precursors, the annealing time, and the use of $CoCl_2$ and sodium hypophosphite as Co and P precursors, respectively. Considering the relationship between the morphology and particle size obtained under different parameter conditions, three different Co_2P species were obtained and analysed electrochemically for glucose detection, revealing evident differences in catalytic activity. In the following sections we evaluate the synthesis conditions, the effect on the catalytic non-enzymatic oxidation of glucose, the kinetics study of the proposed sensors, and the analytical performance for glucose quantification.

2. Materials and methods

2.1. Reagents

All the chemicals used were of analytical grade. Cobalt chloride hexahydrate ($CoCl_2 \bullet 6H_2O$, Aldrich, St. Louis, MO, USA), sodium phosphinate monohydrate ($NaPO_2H_2 \cdot H_2O$, Merck), polyvinyl pyrrolidone ($(C_6H_9NO)n$, PVP, MW = 1,300,000), orthophosphoric acid (H_3PO_4 85%, Merck), N,N dimethylformamide (C_3H_7NO, DMF Merck), hexamethylenediamine ($C_6H_{16}N_2$, Merck), 0.3 and 0.05 μm alumina (Buehler, Uzwil, Switzerland), α-D-glucose ($C_6H_{12}O_6$ Sigma–Aldrich), Nafion (5.0% Aldrich), sodium hydroxide (NaOH, Merck), ethanol (Analytical Grade, Merck), acetone (Analytical Grade, Merck), and ethylenediamine (Merck) were used. For the thermal treatments, H_2 and Ar (Air Liquide, Paris, France) were used. All the electrochemical solutions were prepared with ultrapure water (ρ = 18.2 MΩ cm) from a Millipore-Milli-Q system that was used for preparing all the aqueous solutions.

2.2. Synthesis of Co_2P

Co_2P was prepared according to the method proposed by Peng et al. [34] with modifications, using cobalt chloride ($CoCl_2$) and sodium hypophosphite ($NaPO_2H_2 \bullet H2O$) as precursors (dissolve in Milli-Q water using different molar ratios Co:P = 1.0:1.30, 1.0:1.35, 1.0:1.40, 1.0:1.45, 1.0:1.50, 1.0:1.60 and 1.0:1.75). After stirring for 1 h, the precursors solution was slowly evaporated at 90°C for 8 hours and then left to stand at room temperature until the precursors were obtained. Then, they were ground in an agate mortar. The products were obtained by calcination of the precursors at 600°C for 6 hours in an Ar atmosphere at a heating rate of 5°C/min. For the temperature study, precursors with a molar ratio of Co:P = 1.0:1.40 were calcinated at 500, 600, and 700°C for 6 hours. Similarly, the calcination duration optimization study, the same precursor (Co:P = 1.0:1.40) was calcinated at 600°C for 6 and 12 hours. The products were cooled down to room temperature under flowing Ar and washed repeatedly with Milli-Q water and ethanol. The final product was obtained after drying at 80°C for 12 hours.

2.3. Synthesis of carbon fibre (CF)

The synthesis of carbon fibres was carried out using electrospinning stretching LE-10 Fluidnatec equipment and 10 ml Nipro Luer/lock syringes based on previous work [19]. Briefly, for electrospinning solution preparation, polyvinylpyrrolidone (PVP) (10% w/v of the final 250 mL solution) was mixed with 125 mL of Milli-Q water and stirred. Then, 125 mL of N,N-dimethylformamide (DMF) was added under stirring. Next, 50.0 mmol of orthophosphoric acid 85% H_3PO_4 was added slowly at room temperature. This solution was electrospun using an 800 μL/hour flow, 18 kV as the voltage and 20 cm as the distance between the needle and the collector. All the experiments were conducted at room temperature and 70% relative humidity. Once the polymer meshes were obtained, they were dried at 110°C for 12 hours. Then, the stabilization process was carried out at 250°C for 3 hours under an air atmosphere using a ramp of 7°C/min. The samples were left to cool to room temperature, and subsequently, the obtained fibres were calcined at 700°C for 3 hours in an Ar/H_2 flow using a 10°C/min heating rate and cooled to room temperature under an Ar atmosphere.

2.4. Materials characterization

The crystalline structure and purity of the obtained materials were determined via X-ray diffraction (XRD). The X-ray diffraction data were collected at room temperature on a Bruker D8 Advance (R-X: Cu tube (CuKa1 radiation = 1.5604 angstroms) with a nickel filter, linear LynxEye detector, 40 KV/30 mA power, and variable, V20 optics). The spectra were measured in the 2θ range between 10 and 80° (PSD step=0.20; 10.0 sec/step). The analysis of crystalline phases was

performed using the Crystal Impact Match program with the PDF-2 database. Parameter lattices were calculated using STOE XPOW software. The surface morphology was studied using a Thermo-Fisher Scientific INSPECT-F50 high-resolution scanning electron microscope (HR-SEM, FEI, The Netherlands). The compositional study was conducted by energy dispersive spectroscopy (EDX), scanning transmission electron microscopy (STEM), and an Alpine 129 eV ultradry pathfinder (Thermo Fisher Scientific).

2.5. Preparation of the CF/Co_2P-modified glassy carbon electrode (CF/Co_2P/GCEs)

A drop-casting technique was used to modify a glassy carbon electrode (GCE). Dispersions of 2.0 mg/mL of the synthesized materials dissolved in 0.2% Nafion in isopropanol and water were prepared. For the CF/Co_2P composite, the materials were massed with 60 wt% CF, and all the dispersions were sonicated for 1 hour. Before each modification, the electrode was polished in 0.3 and 0.05 μm alumina and then washed with Milli-Q water. Ten microlitres of the dispersion was taken and deposited on the surface of a glassy carbon electrode and then dried at 50°C for 10 minutes.

2.6. Electrochemical measurements

The catalytic activity of the modified electrodes was tested using a typical three-electrode system composed of a bare or modified GCE as working electrode (CH Instrument, Bee Cave, TX, USA, 3 mm diameter), an Ag/AgCl reference electrode in 3 mol/L NaCl (CH Instrument), and an auxiliary platinum wire electrode. A 10 mL-cell was used for the electrochemical experiments, performed with a MultiEmStat potentiostat (Palmsens BV, Houten, The Netherlands). All the electrochemical measurements were carried out in triplicate by immersing the modified electrode in 5.00 mL of 0.100 M NaOH as the supporting electrolyte. Cyclic voltammetry was performed at a scan rate of 50 mVs^{-1} between 0.00 and 0.800 V. Linear sweep voltammetry was performed using a BAS CV 50W potentiostat with a rotating disk at 2000 rpm and a scan rate of 5.00 mVs^{-1} in a deoxygenated 0.100 M NaOH solution with a 1.00 mM glucose solution. For the selection of the working potential, hydrodynamic voltammetries were carried out between 0.500 and 0.600 V, aiming to find the potential with the highest current and low measurement dispersion. Finally, the analytical studies were conducted using amperometry at 0.600 V.

3. Results

3.1. Physical and structural characterization of the synthetized materials

The crystalline structure of the Co_2P species and byproducts obtained were determined via X-ray diffraction (XRD). The Co_2P synthesis conditions, such as the molar ratio between the Co:P precursors, calcination temperature and time, were studied. These parameters are relevant in phosphorization treatments since it is possible to form many byproducts by the phosphine gas (PH_3) released during this process [32]. Based on the mechanism process reported for Ni_2P [33], the reactions that could be involved in the thermal decomposition process using $CoCl_2$ and NaH_2PO_2 as precursors in an Ar atmosphere can be explained as follows:

Formation of the intermediate product:

$$2NaH_2PO_2 + CoCl_2 \rightarrow 2NaCl + Co(H_2PO_2)_2 \quad (1)$$

Dismutation of the intermediate product and release of PH_3 gas:

$$Co(H_2PO_2)_2 \rightarrow PH_3 + CoHPO_4 \quad (2)$$

Considering that no mechanistic studies have been reported to clarify the conversion of $CoHPO_4$ to Co_2P, the formation of Co_2P is attributed to the reaction of $CoHPO_4$ with the previously released PH_3. This process is represented by the following reaction:

$$4PH_3 + 4CoHPO_4 + CoCl_2 \rightarrow 3Co_2P + P + 4H_3PO_4 + 4HCl \quad (3)$$

The formation of PH_3 results in different reactions due to its high reactivity as a reductor agent at temperatures above 300°C [34]. To obtain pure Co_2P, we first evaluated the effect of different molar ratios of $CoCl_2$ to NaH_2PO_2 as precursor, using 600°C and 6 hours as the calcination temperature and time, respectively. The XRD patterns of the materials obtained with Co:P molar ratios varying from 1.0:1.30 to 1.0:1.75 are displayed in Fig. 1A. The results showed that the molar ratio between precursors drastically influence Co_2P and byproduct formation. Characteristic peaks of the Co_2P diffraction pattern and interfering phases corresponding to CoP_2 and $Na_2CoP_2O_7$ were generated at a Co:P molar ratio of 1.0:1.75. When the molar ratio of Co:P was decreased to 1:1.60, 1:1.50, and 1:1.45, the intensity of the CoP_2 and $Na_2CoP_2O_7$ peaks decreased. CoP_2 was no longer observed at molar ratios of Co:P =1.0:1.40 and 1.0:1.35, and finally, the pure Co_2P phase was obtained with no additional planes at a Co:P = 1.0:3.0 molar ratio. Based on the phosphorization mechanism described earlier, the formation of interferents is triggered by an excess of NaH_2PO_2 (Eq. 1), which ultimately leads to the generation of high amounts of PH_3 by dismutation (Eq. 2); as a result, parallel reactions can occur that form byproducts, or the reactions may be incomplete during these syntheses. Based on the previous results, the Co:P ratio = 1.0:1.30 allows the formation of Co_2P without impurities, allowing the phosphorization reactions mentioned in Eqs. (1)–(3) to be completed correctly. The Co_2P species obtained under these conditions were named Co_2P (1). [33,30]

The influence of calcination time was studied at a molar ratio of Co:P = 1:1.4 at 600°C, and the calcination time was varied from 6 to 12 hours. Fig. 1B shows that pure Co_2P was obtained when the calcination time was increased to 12 hours, indicating that the calcination time is a decisive parameter in the formation of pure Co_2P. The Co_2P obtained under these synthetic conditions was named Co_2P (2). Finally, the third parameter evaluated in the synthesis of pure Co_2P was the calcination temperature. Fig. 1C shows the diffractograms obtained using calcination temperatures of 500, 600, and 700°C at a Co:P molar ratio of 1.0:1.40 and after 6 hours of calcination. A greater number of intermediates was detected when 500°C was used, as the intensity of the diffraction peaks corresponding to $Na_2CoP_2O_7$ was greater than that of any other protocol used. When the temperature increased to 600°C, the intensity of the peaks decreased; finally, Co_2P was obtained at 700°C without the presence of planes corresponding to other species. Thus, at this temperature, the reactions involved in the formation of Co_2P are guaranteed to reach completion. The Co_2P obtained under these synthetic conditions was named Co_2P (3).

The diffractograms of the three pure Co_2P species obtained are detailed in Fig. 1D and agree with the Co_2P pattern (PDF2 no. 01-089-3030), corresponding to an orthorhombic crystalline system of space group pnma. The crystallite sizes obtained by the Debye–Scherrer equation and the particle sizes determined by STEM images from a Gaussian-type distribution for the Co_2P species (Fig. S1) are shown in Table 1.

A direct correlation between the crystallites and particle size was observed, and the differences between the synthesis conditions were in the following order: Co_2P (1) < Co_2P (2) < Co_2P (3). The Co_2P (1) and Co_2P (2) particles were compared under the same calcination temperature; therefore, the larger crystallite and particle sizes for Co_2P (2) are attributed to the longer time under heat treatment, which induces greater grain growth. On the other hand, Co_2P (3) had the largest crystallite and particle sizes of the three species obtained; thus, compared to longer sintering times, a higher sintering temperature (700°C) more greatly affects grain growth in these systems [36].

SEM images of Co_2P (1), Co_2P (2), and Co_2P (3) are presented in Fig. 2B–D, respectively. An amorphous morphology can be observed for the synthesized cobalt phosphides. In particular, for Co_2P (1), it is

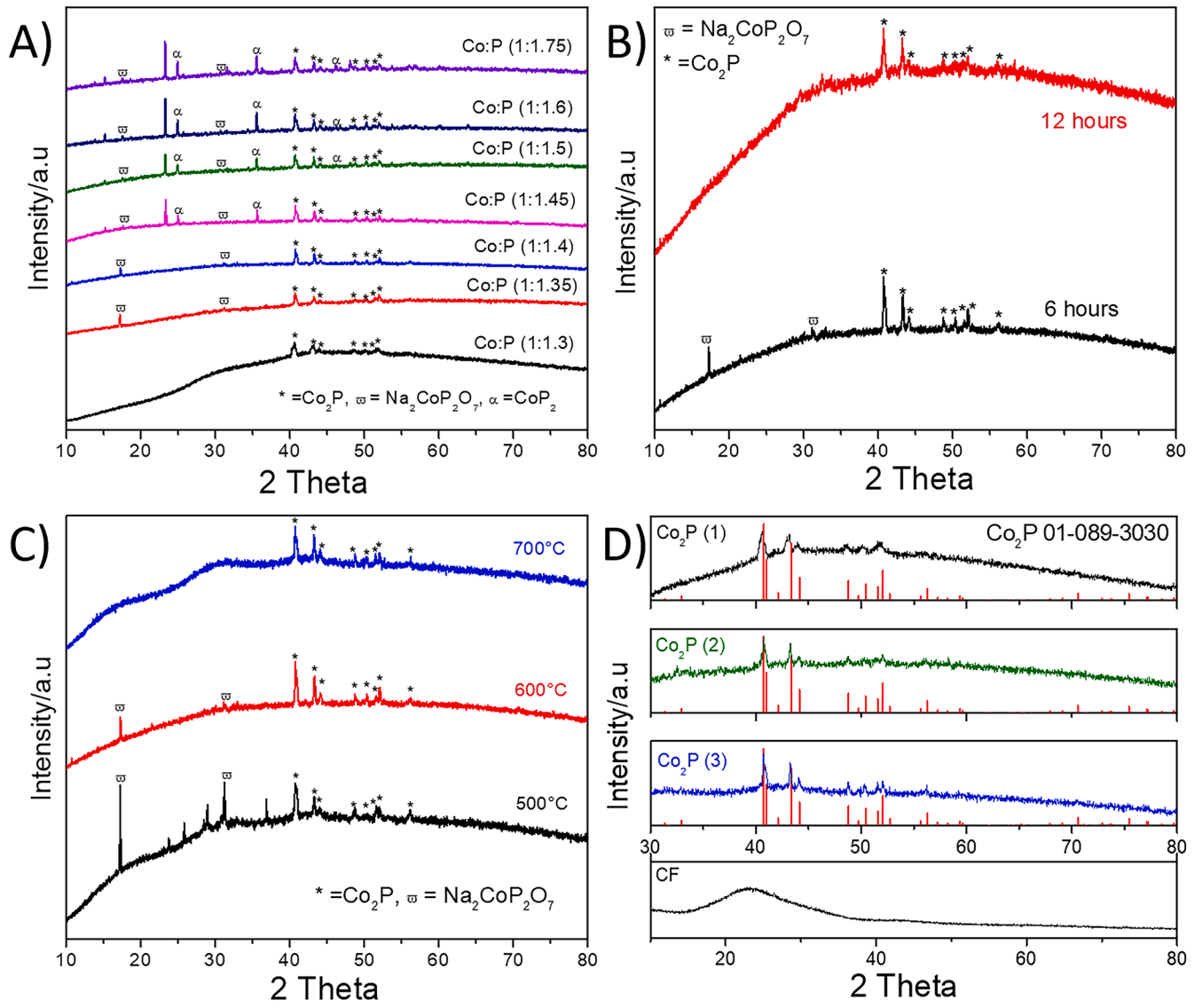

Fig. 1. X-ray diffraction (XRD) results of A) Co_2P synthesized with different molar ratios of $CoCl_2$: NaH_2PO_2 (Co:P) with a calcination time of 6 hours at a temperature of 600°C, B) Co_2P with a molar ratio of Co:P = 1:1.40 with calcination times of 6 and 12 hours at a temperature of 600°C, C) Co_2P with a molar ratio of Co:P = 1:1.40 with calcination times of 6 hours at 500°C, 600°C and 700°C, and D) the obtained Co_2P species and carbon fibre (CF).

Table 1
Synthesis conditions of Co_2P species, average crystal size from the Debye–Scherrer equation, and particle size obtained from STEM images.

Material	Synthesis conditions			Crystallite size (nm)	Particle size (nm)
	Temperature (°C)	Calcination time (h)	Molar ratio (Co:P)		
Co_2P (1)	600	6	1.0:1.3	13.6 ± 1.1	44.7 ± 23.7
Co_2P (2)	600	12	1.0:1.4	26.2 ± 3.5	78.1 ± 32.9
Co_2P (3)	700	6	1.0:1.4	35.3 ± 6.1	154.6 ± 96.6

possible to observe particles with a flower/urchin-like morphology (Fig. 2B). Morphology that is important in electrocatalytic materials where a high surface is required [24,37].

The particle size of Co_2P obtained is changed by the calcination time and temperature, and an increase in the time and temperature of synthesis leads to appreciable grain growth, which was observed for Co_2P (2) and Co_2P (3) in comparison with Co_2P (1).

The distribution of cobalt and phosphorus in each synthesized Co_2P species was obtained from EDX analysis (Fig. 2S). In all cases, a homogeneous distribution of cobalt and phosphorus was observed.

Concerning the carbon material, Fig. 1D shows the CF diffraction pattern, in which a diffraction peak occurs at approximately 2theta= 24°, which is characteristic of carbon materials [38,39]. A smooth fibre morphology without visible pores or cracks can be observed in the SEM image in Fig. 2A. This is related to the optimized electrospinning and heat treatment parameters involved in the synthesis, through which carbon fibres can be formed without apparent defects, as described in previous work by Brito T.P. [19]. In addition, an advantage of the electrospinning technique is that the fibre diameter is controlled [40]; in this case, an average diameter of 123 nm was obtained.

3.2. Electrocatalytic performance against glucose

The electrochemical behaviour of the Co_2P species was examined using cyclic voltammetry in a potential range of 0.00 to 0.800 V in 0.100 M NaOH solution at a scan rate of 50.0 mVs^{-1}. Fig. 3A shows the cyclic

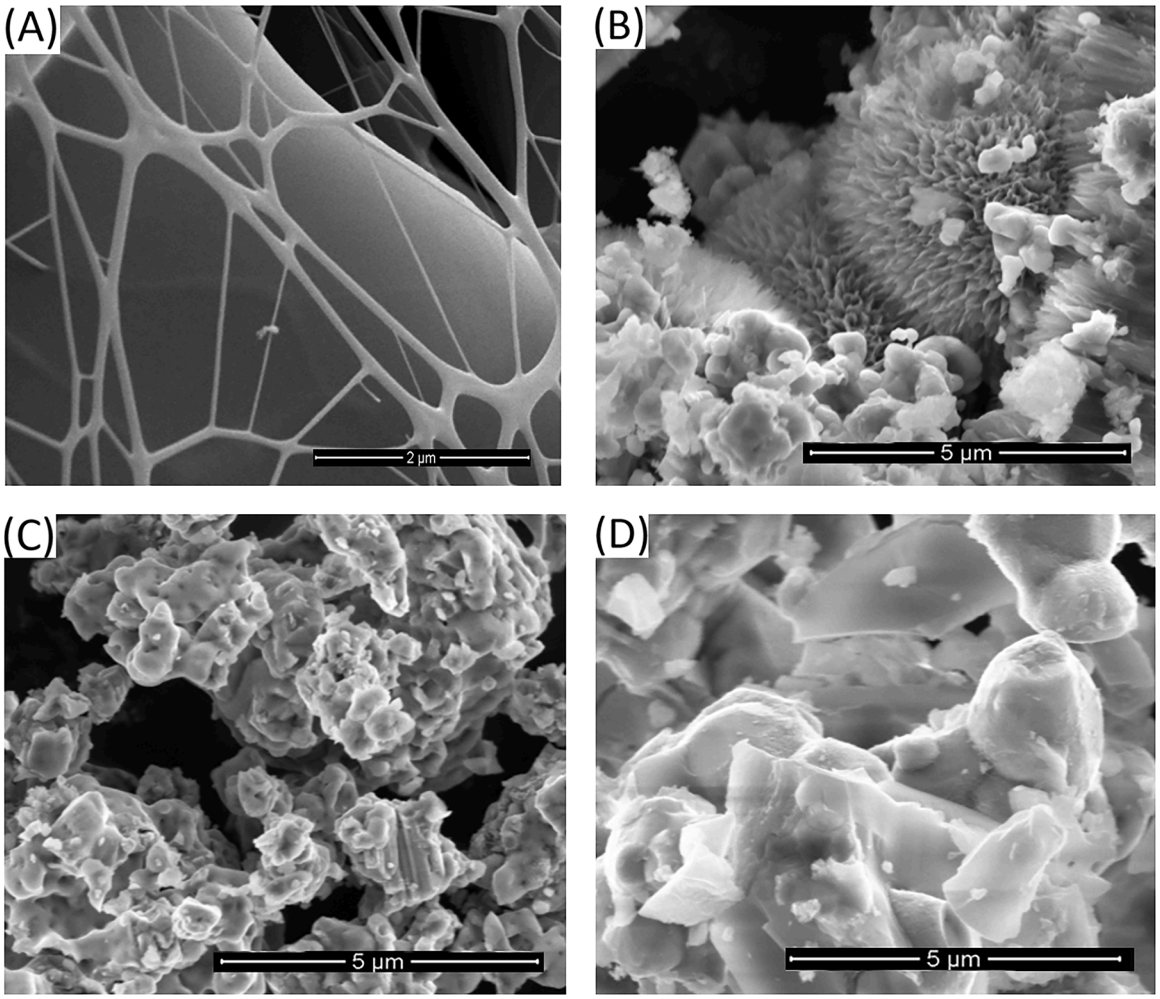

Fig. 2. SEM images of A) carbon fibre (CF), B) Co_2P (1), C) Co_2P (2), and D) Co_2P (3).

voltammograms of pure Co_2P-modified GCE electrodes, for which a well-defined oxidation peak appears at approximately 0.400 V for the GCE/Co_2P (1) electrode. Considering that at the unmodified GCE there were no significant redox peaks (not shown) and the reported studies on the electrochemistry of cobalt phosphides, such as Co_2P[40] and CoP [40], this process can be assigned to the oxidation of $Co^{\delta+}$ present in Co_2P to Co^{3+} (CoOOH species) in an alkaline medium as follows:

$$Co^{\delta+} + nOH^- + H_2O \rightarrow CoOOH + ne^- \quad (4)$$

For the GCE/Co_2P (2)- and GCE/Co_2P (3)-modified electrodes, the anodic current associated with the oxidation of $Co^{\delta+}$ is very low compared to that of GCE/Co_2P (1), and in the case of Co_2P (3), the process occurs at higher potentials. Thus, the formation of CoOOH species via Eq, (4) varies drastically depends on the synthesis method by which Co_2P was obtained, possibly due to the smaller particle size of Co_2P (1) compared to the other Co_2P species; this smaller size contributes to greater wettability and the subsequent formation of CoOOH active species on the electrode surface. As CoOOH is the electrocatalytic species necessary for glucose oxidation, Co_2P (1) was chosen for the electroanalytic evaluation.

The cyclic voltammograms of Co_2P- and CF/Co_2P-modified electrodes in the absence and presence of 1.00 mM glucose are presented in Fig. 3B. The process described in Eq, (4) related to the formation of CoOOH occurred at both electrodes. When the CF/Co_2P composite was used, a broader oxidation peak was obtained, which was attributed to greater electron flow; in addition, a small positive shift in the anodic peak potential compared to that of Co_2P was observed. This behaviour was also observed when CF/Ni_2P composites were evaluated [41] and is related to possible adsorption mechanisms on the surface of modified electrodes containing CFs. A second process at approximately 0.600 V was observed in the presence of glucose for both materials. Considering that CF does not undergo any significant redox reaction in the presence of glucose, this process is attributed to the oxidation of CoOOH to CoO_2 according to the following reaction [40,26]:

$$CoOOH + OH^- \rightarrow CoO_2 + H_2O + e^- \quad (5)$$

For both electrodes, the addition of glucose induces an increase in the oxidation current at a peak of approximately 0.600 V, while the current peak near 0.400 V remains constant or decreases. The same effect was observed in Fig. 4A for the CF/Co_2P composite after glucose was successively added. Thus, the oxidation of glucose to gluconolactone is catalysed by the conversion of CoO_2 to CoOOH [41,42] as follows:

$$CoO_2 + \text{glucose} + H_2O \rightarrow CoOOH + OH^- + \text{glucolactone} \quad (6)$$

Cyclic voltammetry (CV) experiments indicate that the CF/Co_2P composite has a greater response to current density against glucose oxidation than that of Co_2P, which is attributed to the high electronic conduction properties of CF as well as the increase in electroactive area due to the high porosity of CF. Therefore, CF together with Co_2P improved the electrocatalytic properties of the material towards the oxidation of glucose (Fig. 4A); thus, the glucose detection performance of CF was further studied.

Fig. 4B shows the CV curves of CF/Co_2P at different scan rates in the

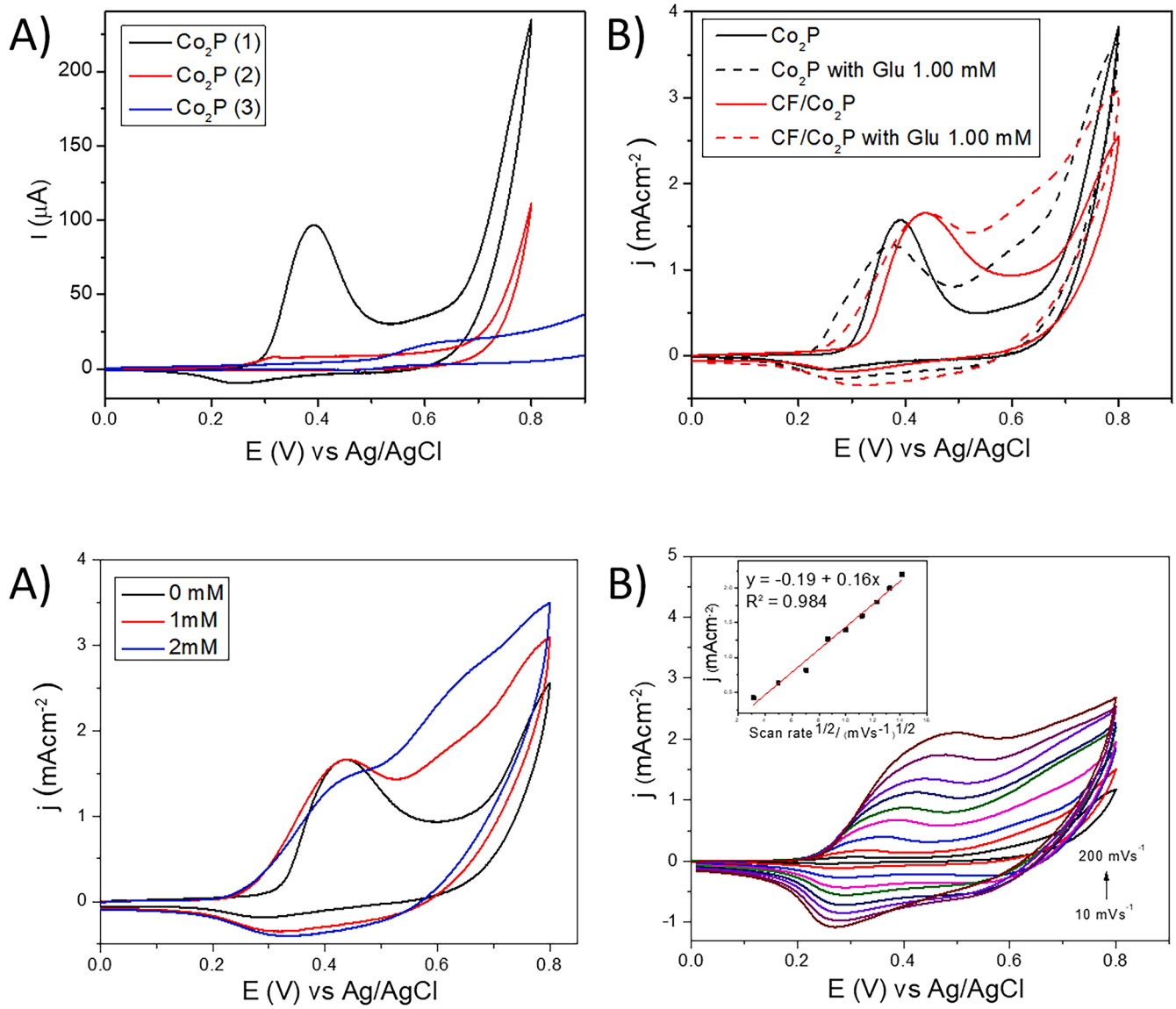

Fig. 3. Cyclic voltammetry (CV) of modified electrodes: A) GCE/Co_2P (1), GCE/Co_2P (2), and GCE/Co_2P (3). B) GCE/Co_2P (1) and GCE/CF/Co_2P (1) in the absence and presence of 1.00 mM glucose. Conditions: potential range from 0.00 to 0.800 V in 0.100 M NaOH.

presence of 1.00 mM glucose in a 0.100 M NaOH solution. As the scan rate increases, the anodic peak shows a slight shift to positive potentials, while the cathodic peak shifts to negative potentials. This indicates that the redox reactions involved in glucose oxidation (Eqs. 4 and 5) correspond to a quasi-reversible process. In addition, a linear relationship was observed between the current density and the square root of the scan rate (insert of Fig. 4B), indicating that the glucose oxidation process was mainly controlled by diffusion. A linear relationship between the logarithmic plot of the current vs. scan rate was observed with a slope of approximately 0.600. Thus, a mixed mechanism is possible for the CF/Co_2P composite, while for Co_2P, the slope is close to 0.500 (Fig. S5); therefore, the contribution of glucose adsorption on the surface of the CF is attributed to the glucose oxidation process [41].

The electrocatalytic activity for the glucose oxidation reaction of both materials was evaluated using polarization curves. Linear scanning voltammetry (LSV) was performed by rotating disk electrodes (RDEs) in the presence of 1.00 mM glucose in a 0.100 M N_2-saturated NaOH solution using a scan rate of 5.00 mVs^{-1} and 2000 rpm (Fig. 5A).

From the polarization curves, a lower onset potential (409 ± 8) mV can be observed with CF/Co_2P compared to Co_2P alone (425 ± 4) mV, indicating that the glucose oxidation process can occur with a lower energy requirement when CF is used with Co_2P compared to Co_2P alone. Furthermore, higher current densities were obtained for the composite in the presence of glucose. Therefore, the values of the standing wave potential and current response indicate that the most active catalyst is the CF/Co_2P composite. The average Tafel slopes (mV/dec) obtained from Fig. 5B correspond to (114 ± 2) mV /dec and (111.4 ± 0.9) mV/dec for Co_2P and CF/Co_2P, respectively. These slope values are close to 120 mV/dec for both materials, indicating that the redox mechanism is independent of the type of Co_2P-based material used. In addition, a value of approximately 120 mV indicates that the transfer of one electron is the rate-limiting step of the reaction [36,42], corresponding to the formation of the active species, which can be followed by a glucose adsorption step on the electrode.

3.3. *Electroanalytical studies*

After studying the electrocatalytic activity of Co_2P and CF/Co_2P on the oxidation of glucose, we evaluated the analytical performance of the sensors. The applied potential is a crucial parameter to be optimized in amperometric glucose detection. Considering that the oxygen generation reaction (OER) starts close to 0.700 V for Co_2P species [25], the

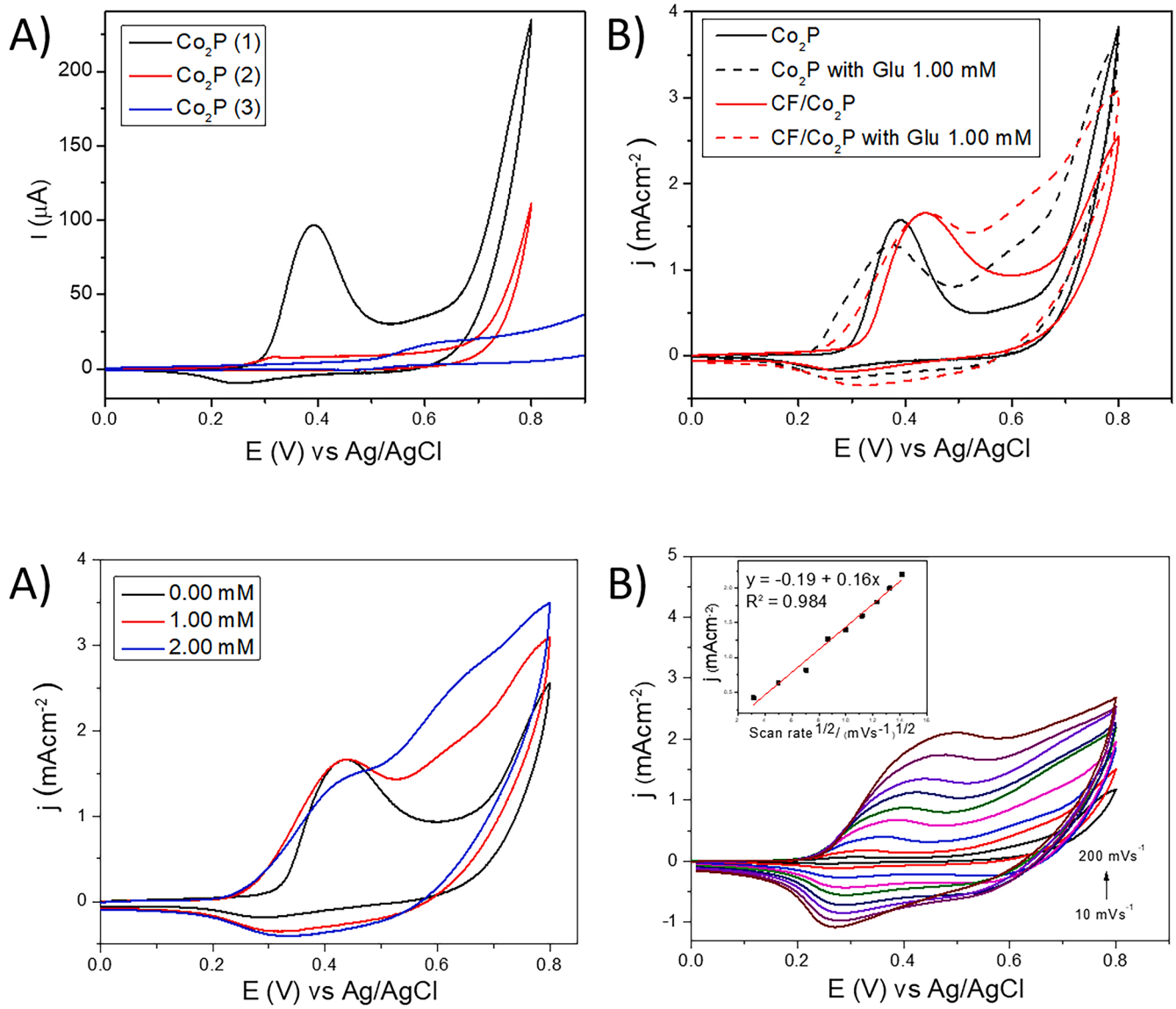

Fig. 4. Cyclic voltammetry (CV) curves of modified GCE/CF/Co_2P electrodes. A) In the absence and presence of 1.00 mM glucose and 2 mM glucose at a scan rate of 50.0 mVs^{-1}. B) In the presence of 1.00 mM glucose at different scan rates between 10 and 200 mVs^{-1}. The corresponding plots of the current density vs. the square root of the scan rate were inserted. Conditions: potential range from 0.00 to 0.800 V in 0.100 M NaOH solution.

response to glucose at GCE/CF/Co_2P electrode was evaluated between 0.500 and 0.600 V. Fig. 6A shows the effect of applied potentials on the amperometric response of CF/Co_2P with successive additions of 20.0 μM glucose in 0.100 M NaOH. The current response gradually increases with increasing potential ranging from 0.500 to 0.600 V. The hydrodynamic voltammogram shown in Fig. 6B reveals that at 0.600 V, the current is 4 times greater than that obtained at 0.500 V, with a small standard deviation; therefore, 0.600 was chosen as the working potential for glucose.

Using 0.600 V as the working potential in 0.100 M NaOH solution, the amperometric response of the modified GCE/CF/Co_2P and GCE/Co_2P electrodes was evaluated (Fig. 7A). In both cases, a fast amperometric response (close to 2 seconds) was observed after glucose addition. The CF/Co_2P composite has the most sensitive response to glucose detection, in accordance with the aforementioned electrochemical characterization results. A linear relationship between the current response and the concentration of glucose was observed for both systems at concentrations ranging from 39.4 to 150 μM (Fig. 7B), reaching sensitivities of 409 $\mu AmM^{-1}cm^{-2}$ and 288 $\mu AmM^{-1}cm^{-2}$ for CF/Co_2P and Co_2P, respectively. These results demonstrated the synergistic effect generated by the combination of CF and Co_2P nanoparticles.

The performance of our GCE/CF/Co_2P sensor is comparable to that of other non-enzymatic glucose sensors, as detailed in Table 2. The analytical parameters for the GCE/CF/Co_2P sensor showed a very similar LOD to most glucose sensors. Some exceptions, such as the cobalt phosphide NPCNT/Co_2P [40], which has a limit of detection (LOD) comparable to that of our electrode, obtaining this material requires the decomposition of triphenylphosphine as a phosphorus precursor at a high temperature of 850°C, which implies a higher synthesis cost compared to the method used in our study. On the other hand, another species of phosphide, such as NiCoP/Ti [43], although it has a slightly lower LOD than our electrode, uses a titanium mesh, which increases the cost of this device. Besides, our sensor shows higher sensitivity than that of most cobalt phosphide-based sensors, such as NPCNT/Co_2P [40]; CoP nanorods [40]; Co-P species, such as phosphates and nickel-cobalt phosphate [44]; other cobalt species; Co_3O_4 nanofibers [45]; and NiCo-LDHb/GNR [46]. The sensitivity of this sensor was greater than that of electrodes based on Co composites with carbon materials, such as Co_2P/NPCNT and NiCo-LDHb/GNR, demonstrating that CF shows great potential for use in general sensors.

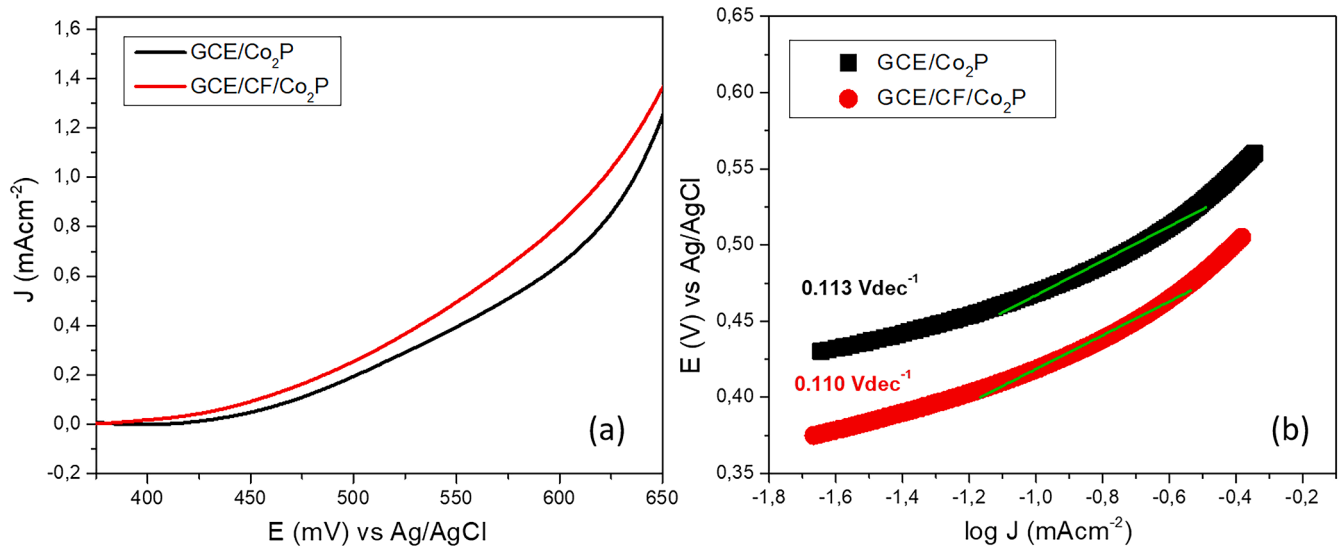

Fig. 5. A) Polarization curves of modified electrodes (GCE/Co_2P and GCE/CF/Co_2P) in the presence of 1.00 mM glucose at a scan rate of 50.0 mVs^{-1} in 0.100 M NaOH solution and a rotation rate of 2000 rpm. B) Tafel slopes obtained from the polarization curves.

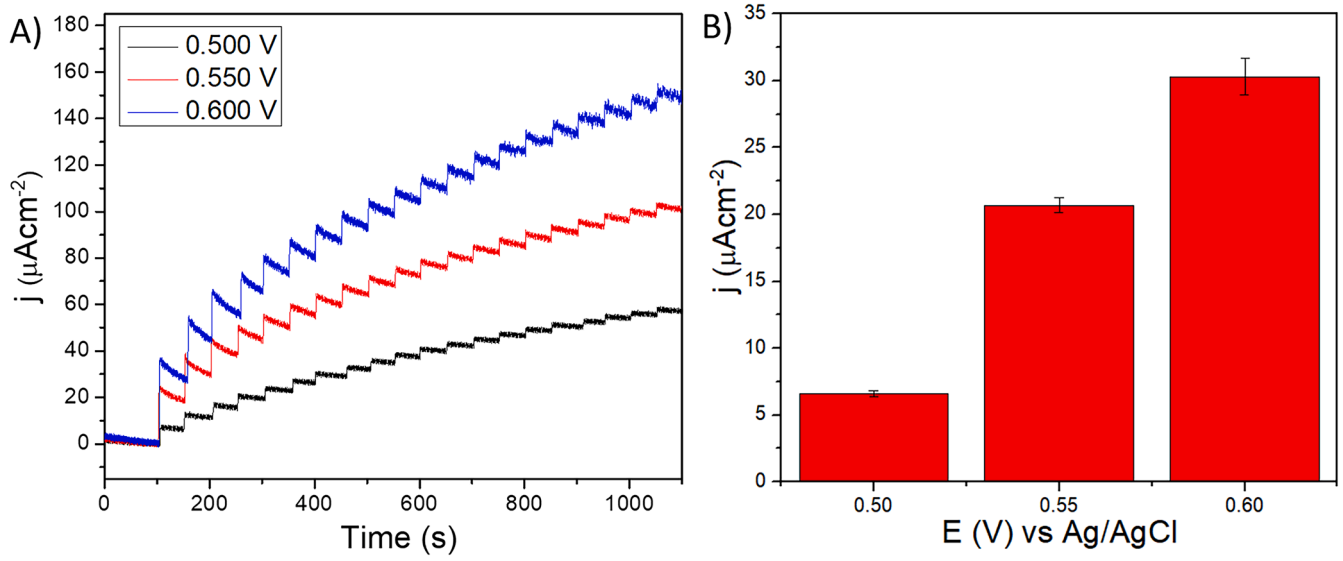

Fig. 6. A) Amperometry of the GCE/CF/Co_2P electrode to successive additions of 20.0 µM glucose in 0.100 M NaOH solution at different potentials vs. Ag/AgCl electrode. B) Hydrodynamic voltammetry at different potentials in the presence of 20.0 µM glucose in 0.100 M NaOH solution, corresponding to three measurements.

The analysis of the catalytic performance of phosphides of other transition metals such as; Ni_5P_4 [47], PdNPs/Ni-P [48], Co_3O_4/CuO@-CoMnP [49], and NiCoP [43] is seen in Table 2. In this sense, the porous flower-like Ni_5P_4, PdNPs/Ni-P nanosheets present a lower sensitivity compared to our sensor. On the other hand, a higher LOD was obtained for the case of the CoMnP-based composite. Another type of P-based material is transition metal phosphates, which have been shown to be electroactive materials for glucose detection; NH_4NiPO_4 nanorods [50], $Co_3(PO_4)_2$ [51], $Ni_3(PO_4)_2$/CSs [52]. With the exception of $Ni_3(PO_4)_2$/CSs in the range of 5.0 µM-2.5 mM, it is interesting to note that all these materials offer a clearly lower sensitivity than our sensor. As they also offer a higher glucose detection limit. In this way, it is generally observed that metal phosphides offer greater catalytic performance than the mentioned phosphates.

On the other hand, unlike most of the sensors mentioned in Table 2, this sensor has a linear range that make it applicable in physiological environments in which the glucose concentration is low, such as in saliva and sweat [53,54], demonstrating to be promissory for the development of new non-invasive sensors.

Selectivity is also an important parameter used to assess the performance of sensors and their ability to prevent interferences from endogenous species. Therefore, the selectivity of the GCE/FC/Co_2P sensor for glucose was investigated by studying the effects of different species that normally coexist with glucose in physiological samples, such as urea, uric acid, ascorbic acid, lactose, and NaCl [53,56]. Amperometric responses of the sensor to the addition of 50.0 µM glucose followed by interferent addition at a concentration of 50.0 µM in 0.100 M NaOH solution at 0.600 V (Fig. S6) shows the expected fast and clear response to glucose, while additions of urea and NaCl does not produce an appreciable increase in current. On the other hand, uric acid, ascorbic acid and lactose produce a low degree of interference at equimolar concentrations, with 7, 15 and 23% (uric acid, ascorbic acid and lactose) of the initial glucose current observed, respectively. In addition, in the presence of interferents in solution, a considerable current response was observed when glucose was added a second time, reaching 80% of the initial current. As the normal glucose level in humans is generally at

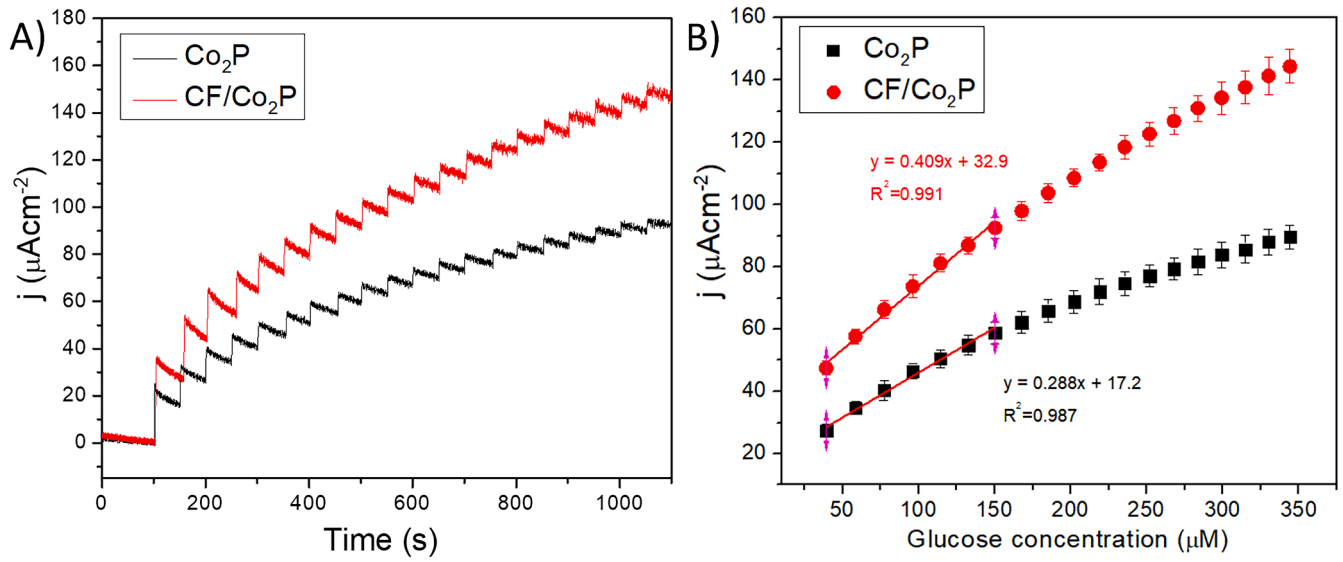

Fig. 7. A) Amperometric response of the modified electrodes to successive additions of 20.0 μM glucose in 0.100 M NaOH solution at a potential of 0.600 V vs. Ag/AgCl electrode. B) Current response as a function of glucose concentration, corresponding to three measurements.

Table 2
Sensing performance comparison of GCE/CF/Co_2P with other nonenzymatic glucose sensors.

Sensor	Sensitivity ($\mu AmM^{-1}cm^{-2}$)	Concentration range	LOD (μM)	Ref
GCE/NPCNT[a]/Co_2P	338.8	1.00 mM – 7.00 mM	0.88	[40]
GCE/CoP nanorods	116.8	500 μM – 5.50 mM	9.0	[40]
GCE/NiCoP nanocages	6115	5.00 μM – 7.00 mM	0.36	[55]
GCE/GNR[b]/NiCo-LDH[c]	344	5.00 μM – 0.80 mM	0.60	[46]
GCE/Co_3O_4 nanofibers	36.25	Up to 2.04 mM	0.97	[45]
GCE/Nickel-cobalt phosphate	302.9	2.00 μM – 4.47 mM	0.40	[44]
GCE/ Ni_5P_4	149.6	2 μM – 5.3 mM	0.70	[47]
PdNPs[d]/Ni-P nanosheets	242.5	2 μM – 4.65 mM	3.00	[48]
Co_3O_4/ CuO@CoMnP	2445	0.01 mM – 0.55 mM	11.4	[49]
	1774	0.55 mM – 3.03 mM		
NiCoP/Ti	14586	1.0 mM –10 mM	0.13	[43]
NH_4NiPO_4 nanorods	459.4	5.0 μM – 2100 μM	0.50	[50]
	250.2		6.0	
$Co_3(PO_4)_2$	251.9	0.009 mM – 1.16mM	3.9	[51]
	139.4	1.16 mM – 4.16mM		
$Ni_3(PO_4)_2$/CSs[e]	480.1	5.0 μM – 2.5 mM	1.67	[52]
	219.8	2.5 mM – 7.5mM		
GCE/CF/Co_2P	409.8	39.4 μM – 150.4 μM	0.97	This work
GCE/Co_2P	288.5	39.4 μM – 150.4 μM	1.04	This work

[a] NPCNT= N,P dual doped carbon nanotubes
[b] GNRs= graphene nanoribbons
[c] LDH= layered double hydroxide
[d] PdNPs= palladium nanoparticles
[e] CSs= composite microspheres

least ten times higher than that in common interferents [11], the GCE/CF/Co_2P sensor is highly selective against glucose detection even in the presence of interferents in equimolar ratios.

4. Conclusions

In summary, pure Co_2P could be generated under three different synthesis conditions in which the molar composition of the Co and P precursors, temperature and calcination time were varied. The Co_2P (1) species presents superior catalytic activity towards GOR, characterized by the smallest particle size and the presence of a flower/urchin-like morphology. The experimental conditions for Co_2P synthesis were a molar ratio of Co:P precursors of 1.0:1.30 and calcination at 600°C for 6 hours below the Ar atmosphere. As an alternative to prevent impurities formation during the synthesis of Co_2P without hindering electrocatalytic activity, longer calcination times or temperatures can be applied. Synergy occurs between the carbon fibres and Co_2P for electrocatalysis via the glucose oxidation reaction, with Tafel slopes close to 120 mV/dec; therefore, the transfer of one electron is the rate-limiting step of the reaction. Finally, the GCE/FC/Co_2P electrode is sensitive and selective for glucose detection without interference from molecules usually present in physiological fluids, and is competitive compared with other non-enzymatic glucose sensors based on cobalt phosphides.

CRediT authorship contribution statement

Tania P. Brito: Writing – original draft, Methodology, Investigation, Formal analysis, Conceptualization. **Nicole Butto-Miranda:** Methodology, Investigation. **Andrónico Neira-Carrillo:** Methodology, Investigation, Conceptualization. **Claudia Yáñez:** Methodology, Funding acquisition, Formal analysis. **Soledad Bollo:** Writing – review & editing, Project administration, Methodology, Funding acquisition, Formal analysis, Conceptualization. **Domingo Ruíz-León:** Writing – review & editing, Methodology, Funding acquisition, Formal analysis, Conceptualization.

Declaration of competing interest

The authors declare that they have no known competing financial interests or personal relationships that could have appeared to influence the work reported in this paper.

Data availability

No data was used for the research described in the article.

Funding

This research was funded by ANID-Fondecyt-Chile Grants (1200828, 1211518, 1200592 and 1211345), ANID National Doctoral Scholarship Chile (21200699), and ANID-FONDAP-Chile (15130011 and 1523A0008).

Supplementary materials

Supplementary material associated with this article can be found, in the online version, at doi:10.1016/j.snr.2024.100235.

References

[1] H. Zafar, A. Channa, V. Jeoti, G.M. Stojanović, Comprehensive review on wearable sweat-glucose sensors for continuous glucose monitoring, Sensors 22 (2) (2022) 1–35, https://doi.org/10.3390/s22020638.
[2] Y. Du, X. Zhang, P. Liu, D.G. Yu, R. Ge, Electrospun nanofiber-based glucose sensors for glucose detection, Front. Chem. 10 (August) (2022) 1–31, https://doi.org/10.3389/fchem.2022.944428, no., pp.
[3] A. Fosch, S. Zagmutt, N. Casals, R. Rodríguez-Rodríguez, New insights of sf1 neurons in hypothalamic regulation of obesity and diabetes, Int. J. Mol. Sci. 22 (12) (2021) 1–22, https://doi.org/10.3390/ijms22126186.
[4] S. Radhakrishnan, S. Lakshmy, S. Santhosh, N. Kalarikkal, B. Chakraborty, C. S. Rout, Recent developments and future perspective on electrochemical glucose sensors based on 2D materials, Biosens. (Basel) 12 (7) (2022), https://doi.org/10.3390/bios12070467.
[5] L. Theuer, M. Lehmann, S. Junne, P. Neubauer, M. Birkholz, Micro-electromechanical affinity sensor for the monitoring of glucose in bioprocess media, Int. J. Mol. Sci. 18 (6) (2017), https://doi.org/10.3390/ijms18061235.
[6] H. Teymourian, A. Barfidokht, J. Wang, Electrochemical glucose sensors in diabetes management: an updated review (2010-2020), Chem. Soc. Rev. 49 (21) (2020) 7671–7709, https://doi.org/10.1039/d0cs00304b.
[7] X. Wu, P. Wu, M. Gu, J. Xue, Ratiometric fluorescent probe based on AuNCs induced AIE for quantification and visual sensing of glucose, Anal. Chim. Acta 1104 (2020) 140–146, https://doi.org/10.1016/j.aca.2020.01.004.
[8] H.A.J. Al Lawati, J. Hassanzadeh, Dual-function 2D cobalt metal-organic framework embedded on paper as a point-of-care diagnostic device: Application for the quantification of glucose, Anal. Chim. Acta 1139 (2020) 15–26, https://doi.org/10.1016/j.aca.2020.09.026.
[9] X. Zhang, et al., High sensitivity electrochemiluminescence sensor based on the synergy of ZIF-7 and CdTe for determination of glucose, Microchemical Journal 177 (January) (2022) 107254, https://doi.org/10.1016/j.microc.2022.107254 no. p.
[10] N. Rasitanon, K. Veenuttranon, H. Thandar Lwin, K. Kaewpradub, T. Phairatana, I. Jeerapan, Redox-mediated gold nanoparticles with glucose oxidase and egg white proteins for printed biosensors and biofuel cells, Int. J. Mol. Sci. 24 (5) (2023), https://doi.org/10.3390/ijms24054657.
[11] M.H. Hassan, C. Vyas, B. Grieve, P. Bartolo, Recent advances in enzymatic and non-enzymatic electrochemical glucose sensing, Sensors 21 (14) (2021), https://doi.org/10.3390/s21144672.
[12] S. Vaidyanathan, J.Y. Cherng, A.C. Sun, C.Y. Chen, Bacteria-templated NiO nanoparticles/microstructure for an enzymeless glucose sensor, Int. J. Mol. Sci. 17 (7) (2016), https://doi.org/10.3390/ijms17071104.
[13] M. Wei, et al., Electrochemical non-enzymatic glucose sensors: recent progress and perspectives, Chem. Commun. 56 (93) (2020) 14553–14569, https://doi.org/10.1039/d0cc05650b.
[14] D.W. Hwang, S. Lee, M. Seo, T.D. Chung, Recent advances in electrochemical non-enzymatic glucose sensors – a review, Anal. Chim. Acta 1033 (2018) 1–34, https://doi.org/10.1016/j.aca.2018.05.051.
[15] Z. Yin, et al., Mingled MnO_2 and Co_3O_4 binary nanostructures on well-aligned electrospun carbon nanofibers for nonenzymatic glucose oxidation and sensing, Cryst. Grow. Des. 21 (3) (2021) 1527–1539, https://doi.org/10.1021/acs.cgd.0c01299.
[16] S. Guo, et al., A facile and sensitive electrochemical sensor for non-enzymatic glucose detection based on three-dimensional flexible polyurethane sponge decorated with nickel hydroxide, Anal. Chim. Acta 1109 (2020) 130–139, https://doi.org/10.1016/j.aca.2020.02.037, no. xxxx, pp.
[17] Z. Lu, et al., N-doped carbon dots regulate porous hollow nickel-cobalt sulfide: High-performance electrode materials in supercapacitor and enzymeless glucose sensor, J. Power. Source. 516 (October) (2021) 230685, https://doi.org/10.1016/j.jpowsour.2021.230685 no.p.
[18] J. Chen, et al., Non-enzymatic glucose sensor based on nickel nitride decorated nitrogen doped carbon spheres (Ni_3N/NCS) via facile one pot nitridation process, J. Alloy. Compd. 797 (2019) 922–930, https://doi.org/10.1016/j.jallcom.2019.05.234.
[19] T.P. Brito, N. Butto-Miranda, A. Neira-Carrillo, S. Bollo, D. Ruíz-León, Synergistic effect of composite nickel phosphide nanoparticles and carbon fiber on the enhancement of salivary enzyme-free glucose sensing, Biosensor. (Basel) 13 (1) (2022) 49, https://doi.org/10.3390/bios13010049, no.p.
[20] L. He, et al., High performance of non-enzymatic glucose biosensors based on the design of microstructure of Ni_2P/Cu_3P nanocomposites, Appl. Surf. Sci. 593 (December 2021) 2022, https://doi.org/10.1016/j.apsusc.2022.153395.
[21] J.F. Callejas, C.G. Read, C.W. Roske, N.S. Lewis, R.E. Schaak, Synthesis, characterization, and properties of metal phosphide catalysts for the hydrogen-evolution reaction, Chem. Mater. 28 (17) (2016) 6017–6044, https://doi.org/10.1021/acs.chemmater.6b02148.
[22] H. Zhang, et al., Refined alteration of active sites via O modification on CoP/Co_2P@Carbon hetero-structural catalyst for hydrogen generation, Appl. Catal. B 325 (May 2023) 122324, https://doi.org/10.1016/j.apcatb.2022.122324.
[23] J. Li, et al., Surface modulation of 3D porous CoNiP nanoarrays in situ grown on nickel foams for robust overall water splitting, Int. J. Mol. Sci. 23 (10) (2022), https://doi.org/10.3390/ijms23105290.
[24] X. Chen, M. Cheng, D. Chen, R. Wang, Shape-controlled synthesis of Co_2P nanostructures and their application in supercapacitors, ACS. Appl. Mater. Interface. 8 (6) (2016) 3892–3900, https://doi.org/10.1021/acsami.5b10785.
[25] S.H. Ahn, A. Manthiram, Cobalt phosphide coupled with heteroatom-doped nanocarbon hybrid electroctalysts for efficient, long-life rechargeable zinc–air batteries, Small. 13 (40) (2017), https://doi.org/10.1002/smll.201702068.
[26] A. Meng, et al., Bimetal nickel–cobalt phosphide directly grown on commercial graphite substrate by the one-step electrodeposition as efficient electrocatalytic electrode, Progr. Nat. Sci.: Mater. Int. 30 (4) (2020) 461–468, https://doi.org/10.1016/j.pnsc.2020.08.003.
[27] L. Xie, A.M. Asiri, X. Sun, Monolithically integrated copper phosphide nanowire: an efficient electrocatalyst for sensitive and selective nonenzymatic glucose detection, Sens. Actuat. B Chem. 244 (2017) 11–16, https://doi.org/10.1016/j.snb.2016.12.093.
[28] Y. Liu, et al., Cobalt phosphide nanowire array as an effective electrocatalyst for non-enzymatic glucose sensing, J. Mater. Chem. B 5 (10) (2017) 1901–1904, https://doi.org/10.1039/c6tb02882a.
[29] C. Hou, X. Zhang, L. Wang, F. Zhang, X. Huang, Z. Wang, A buckypaper decorated with CoP/Co for nonenzymatic amperometric sensing of glucose, Microchimica Acta 187 (2) (2020) 1–8, https://doi.org/10.1007/s00604-019-4076-3.
[30] D. Das, A. Das, M. Reghunath, K.K. Nanda, Phosphine-free avenue to Co_2P nanoparticle encapsulated N,P co-doped CNTs: a novel non-enzymatic glucose sensor and an efficient electrocatalyst for oxygen evolution reaction, Green Chem. 19 (5) (2017) 1327–1335, https://doi.org/10.1039/c7gc00084g.
[31] Y. Shi, B. Zhang, Recent advances in transition metal phosphide nanomaterials: synthesis and applications in hydrogen evolution reaction, Chem. Soc. Rev. 45 (6) (2016) 1529–1541, https://doi.org/10.1039/c5cs00434a.
[32] Q. Guan, W. Li, A novel synthetic approach to synthesizing bulk and supported metal phosphides, J. Catal. 271 (2) (2010) 413–415, https://doi.org/10.1016/j.jcat.2010.02.031.
[33] Q. Guan, W. Li, M. Zhang, K. Tao, Alternative synthesis of bulk and supported nickel phosphide from the thermal decomposition of hypophosphites, J. Catal. 263 (1) (2009) 1–3, https://doi.org/10.1016/j.jcat.2009.02.008.
[34] W. Peng, et al., Co2P: A facile solid state synthesis and its applications in alkaline rechargeable batteries, J. Alloy. Compd. 511 (1) (2012) 198–201, https://doi.org/10.1016/j.jallcom.2011.09.029.
[35] B. Pradhan, et al., Shape-controlled cobalt phosphide nanoparticles as volatile organic solvent sensor, J. Mater. Chem. C. Mater. 4 (22) (2016) 4967–4977, https://doi.org/10.1039/c6tc00949b.
[36] A.S. Danial, M.M. Saleh, S.A. Salih, M.I. Awad, On the synthesis of nickel oxide nanoparticles by sol-gel technique and its electrocatalytic oxidation of glucose, J. Power. Source. 293 (2015) 101–108, https://doi.org/10.1016/j.jpowsour.2015.05.024.
[37] A. Lu, et al., Synthesis of Co2P/graphene nanocomposites and their enhanced properties as anode materials for lithium ion batteries, J. Power. Source. 295 (2015) 329–335, https://doi.org/10.1016/j.jpowsour.2015.06.154.
[38] T.S. Bae, E. Shin, J.S. Im, J.G. Kim, Y.S. Lee, Effects of carbon structure orientation on the performance of glucose sensors fabricated from electrospun carbon fibers, J. Non. Cryst. Solid. 358 (3) (2012) 544–549, https://doi.org/10.1016/j.jnoncrysol.2011.11.002.
[39] J. Saravanan, et al., Flower-like CuO/NiO nanostructures decorated activated carbon nanofiber membranes for flexible, sensitive, and selective enzyme-free glucose detection, J. Mater. Sci.: Mater. Electron. 32 (20) (2021) 24775–24789, https://doi.org/10.1007/s10854-021-06927-x.
[40] Q.Q. Sun, M. Wang, S.J. Bao, Y.C. Wang, S. Gu, Analysis of cobalt phosphide (CoP) nanorods designed for non-enzyme glucose detection, Analyst 141 (1) (2016) 256–260, https://doi.org/10.1039/c5an01928a.
[41] H. Chen, et al., Co-P decorated nanoporous copper framework for high performance flexible non-enzymatic glucose sensors, J. Electroanalyt. Chem. 841 (February) (2019) 119–128, https://doi.org/10.1016/j.jelechem.2019.04.036, no.
[42] A.M. Ghonim, B.E. El-Anadouli, M.M. Saleh, Electrocatalytic glucose oxidation on electrochemically oxidized glassy carbon modified with nickel oxide nanoparticles, Electrochim. Acta 114 (2013) 713–719, https://doi.org/10.1016/j.electacta.2013.10.115.
[43] Z. Wang, et al., Ternary NiCoP nanosheet array on a Ti mesh: a high-performance electrochemical sensor for glucose detection, Chem. Commun. 52 (100) (2016) 14438–14441, https://doi.org/10.1039/C6CC08078B.
[44] Y. Shu, B. Li, J. Chen, Q. Xu, H. Pang, X. Hu, Facile synthesis of ultrathin nickel–cobalt phosphate 2D nanosheets with enhanced electrocatalytic activity for glucose oxidation, ACS. Appl. Mater. Interface. 10 (3) (Jan. 2018) 2360–2367, https://doi.org/10.1021/acsami.7b17005.

[45] Y. Ding, Y. Wang, L. Su, M. Bellagamba, H. Zhang, Y. Lei, Electrospun Co_3O_4 nanofibers for sensitive and selective glucose detection, Biosens. Bioelectron. 26 (2) (2010) 542–548, https://doi.org/10.1016/j.bios.2010.07.050.
[46] E. Asadian, S. Shahrokhian, A. Iraji Zad, Highly sensitive nonenzymetic glucose sensing platform based on MOF-derived NiCo LDH nanosheets/graphene nanoribbons composite, J. Electroanalyt. Chem. 808 (October 2017) (2018) 114–123, https://doi.org/10.1016/j.jelechem.2017.10.060.
[47] X. Xiao, et al., Porous flower-like Ni5P4 for non-enzymatic electrochemical detection of glucose, Mater. Chem. Phys. 240 (Jan. 2020) 122202, https://doi.org/10.1016/j.matchemphys.2019.122202.
[48] M. Wang, Z. Ma, J. Li, Z. Zhang, B. Tang, X. Wang, Well-dispersed palladium nanoparticles on nickel- phosphorus nanosheets as efficient three-dimensional platform for superior catalytic glucose electro-oxidation and non-enzymatic sensing, J. Colloid. Interface Sci. 511 (Feb. 2018) 355–364, https://doi.org/10.1016/j.jcis.2017.10.008.
[49] L. Naderi, S. Shahrokhian, Metal-organic framework-assisted Co_3O_4/CuO@CoMnP with core-shell nanostructured architecture on Cu fibers for fabrication of flexible wire-typed enzyme-free micro-sensors, Chem. Eng. J. 456 (Jan. 2023) 141088, https://doi.org/10.1016/j.cej.2022.141088.
[50] H. Yin, et al., Urea assistant growth of ammonium nickel phosphate ($NH_4NiPO_4·H_2O$) nanorods for high-performance nonenzymatic glucose sensors, J. Electroanalyt. Chem. 846 (Aug. 2019) 113150, https://doi.org/10.1016/j.jelechem.2019.05.032.
[51] D. Zhang, et al., Facile synthesis of cobalt phosphate hydrate nanosheets with enhanced nonenzymatic glucose sensing, Int. J. Electrochem. Sci. 14 (12) (Dec. 2019) 10541–10548, https://doi.org/10.20964/2019.12.72.
[52] T. Zhan, et al., $Ni_3(PO_4)_2$ nanoparticles decorated carbon sphere composites for enhanced non-enzymatic glucose sensing, J. Alloy. Compd. 786 (May 2019) 18–26, https://doi.org/10.1016/j.jallcom.2019.01.304.
[53] D. Bruen, C. Delaney, L. Florea, D. Diamond, Glucose sensing for diabetes monitoring: recent developments, Sensor. (Switzerl.) 17 (8) (2017) 1–21, https://doi.org/10.3390/s17081866.
[54] E.W. Nery, M. Kundys, P.S. Jeleń, M. Jönsson-Niedziólka, Electrochemical glucose sensing: is there still room for improvement? Anal. Chem. 88 (23) (2016) 11271–11282, https://doi.org/10.1021/acs.analchem.6b03151.
[55] Y. Zhu, Y. Wang, K. Kang, Y. Lin, W. Guo, J. Wang, A nickel–cobalt bimetallic phosphide nanocage as an efficient electrocatalyst for nonenzymatic sensing of glucose, Microchimica Acta 187 (2) (Feb. 2020) 100, https://doi.org/10.1007/s00604-019-4073-6.
[56] X. Niu, X. Li, J. Pan, Y. He, F. Qiu, Y. Yan, Recent advances in non-enzymatic electrochemical glucose sensors based on non-precious transition metal materials: Opportunities and challenges, RSC. Adv. 6 (88) (2016) 84893–84905, https://doi.org/10.1039/c6ra12506a.